



Cite this: *New J. Chem.*, 2021, 45, 8321

Design, synthesis, biological evaluation and molecular modelling of substituted pyrrolo[2,1-a]isoquinolinone derivatives: discovery of potent inhibitors of AChE and BChE†

Oscar Parravicini,^{id a} Emilio Angelina,^{id b} Roque Spinelli,^{id c} Francisco Garibotto,^{id a} Álvaro S. Siano,^{id c} Laura Vila,^{id d} Nuria Cabedo,^{id de} Diego Cortes^{id e} and Ricardo D. Enriz^{id *a}

We report here the design, synthesis and biological evaluation of a new series of substituted pyrrolo[2,1-a]isoquinolin-3-one derivatives, some of which have strong inhibitory activity against both AChE and BChE enzymes. The design of these new inhibitors was carried out taking rivastigmine as the starting structure. Thus, on the basis of an exhausting molecular modeling study using combined techniques (docking, dynamic molecular simulations and QTAIM calculations), we obtained new ligands possessing stronger inhibitory effects than rivastigmine, the reference compound. QTAIM analysis gave us detailed information about the molecular interactions stabilizing the different ligand–enzyme complexes. These calculations showed the importance of the interaction with the CAS esteratic site for the inhibitory effect of these compounds. Nevertheless, they also indicated that the combination of interactions with CAS and strong interactions with the PAS site might be beneficial for the inhibitory effect.

Received 21st January 2021,
Accepted 25th March 2021

DOI: 10.1039/d1nj00345c

rsc.li/njc

1. Introduction

Currently, Alzheimer's disease (AD) is without doubt a very serious problem for our society, but it is even more complex for the near future. About fifty million people are currently living with Alzheimer's disease (AD).¹ According to the latest Center for Disease Control and Prevention (CDC) statistics, while other diseases have decreased like, for example, cardiovascular disorders, those involving AD complications have increased. In addition, not just the patients are involved in this particular and difficult disease. The burden experienced by caregivers is also substantial, affecting their physical and mental wellbeing.^{2,3} Despite its societal impact, AD is underdiagnosed, with relatively

few patients having received a formal diagnosis of AD. Furthermore, despite all research efforts, therapeutic options for AD are very limited. At this time, the only treatments available with clinical evidence to AD patients are the cholinesterase inhibitors (ChEI) donepezil, rivastigmine and galantamine for mild to moderate AD, and memantine (an NMDA receptor antagonist) which has been approved for moderate to severe AD. All four compounds have been rigorously tested in clinical trials and have been proved to improve patients' reported outcomes, that is, cognition, memory, communication and the ability to perform daily activities. However, it is important to remark that the above drugs provide symptomatic treatment for the disease, without strong evidence for disease-modifying properties.⁴ In some countries, tacrine is also available for AD treatment. However, it is a substance with a questionable safety profile and, in fact, it is not involved in general AD therapy.

The principal role of acetylcholinesterase (AChE) is the termination of impulse transmission at cholinergic synapses by the rapid hydrolysis of acetylcholine (ACh);⁵ and one of the earliest and major neurobiological findings in AD is a deficit in cholinergic neurotransmission in the basal forebrain. Thus, the reduction of cortical and CSF cholinergic markers, such as AChE, choline acetyl transferase and ACh itself, is correlated with both the extent of the neuropathology and the severity of the cognitive impairment in Alzheimer's disease and other degenerative diseases.^{6,7} Inhibitors of AChE are the principal

^a Facultad de Química, Bioquímica y Farmacia, Universidad Nacional de San Luis, Instituto Multidisciplinario de Investigaciones Biológicas (IMIBIO-SL), Ejército de los Andes 950, 5700 San Luis, Argentina. E-mail: denriz@unsl.edu.ar

^b Laboratorio de Estructura Molecular y Propiedades, IQUIBA-NEA, Universidad Nacional del Nordeste, CONICET, FaCENA, Av. Libertad 5470, Corrientes 3400, Argentina

^c Laboratorio de Péptidos Bioactivos, Departamento de Química Orgánica, Facultad de Bioquímica y Ciencias Biológicas, Universidad Nacional del Litoral, Santa Fe, Argentina

^d Instituto de Investigación Sanitaria INCLIVA, 46010 Valencia, Spain

^e Departamento de Farmacología, Facultad de Farmacia, Universidad de Valencia, 46100 Burjassot, Valencia, Spain

† Electronic supplementary information (ESI) available. See DOI: 10.1039/d1nj00345c

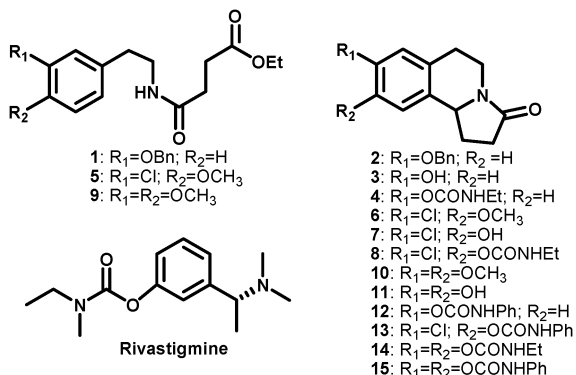


Fig. 1 Structural features of substituted pyrrolo[2,1-*a*]isoquinolin-3-one derivatives and the FDA-approved cholinesterase inhibitor rivastigmine.

therapeutic option for AD; in fact, donepezil, rivastigmine and galantamine are the three inhibitors that are FDA-approved for first-line treatment for AD. Although they share the same mode of action, they differ in terms of their pharmacologic characteristics and route of administration, which can affect their safety and tolerability profile. Rivastigmine, available in both oral and transdermal patch formulations, is a slowly reversible dual inhibitor of acetyl and butyryl cholinesterase, selective for the G1 isoform of acetylcholinesterase, without hepatic metabolism by the CYP-450 system. Considering the very limited number of drugs currently available for therapeutic use in the treatment of AD, it is evident that there is a marked need to find new structures with similar properties to rivastigmine that can be used therapeutically. Our study is focused mainly on such an objective.

Our research group has previously reported the synthesis of 8-substituted and 8,9-disubstituted pyrrolo[2,1-*a*]isoquinolin-3-one derivatives (compounds 1–11, Fig. 1) whose general structures have a slight structural resemblance with rivastigmine.⁸

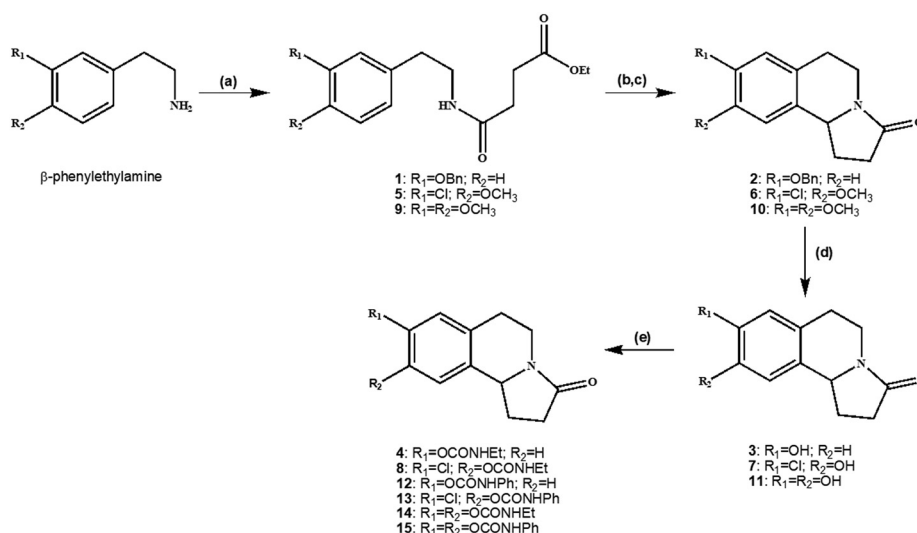
On the other hand, we have recently reported new AChE inhibitors, and in such articles we have conducted molecular modelling studies that have allowed us to understand in some detail the molecular interactions that are involved in the stabilization of different inhibitor–enzyme complexes for this molecular target.^{9–13} In particular, for *N*-benzyl-2-phenylethanamines and carbamate-type ligands we have described the importance of interactions with residues W84, Y121, G118, S122, E199, S200, W279, F330, Y334 and H440 for the stabilization of cholinesterase complexes. Moreover, we carried out a comparative study of AChE and BChE, based on the accessible area within their active sites, which showed that the active site of BChE is larger and more flexible than AChE. Taking advantage of having this information, we asked ourselves if we would be able to design a new structure with inhibitory effects on AChE, taking as a starting structure those previously reported in ref. 8. Thus, we report here the synthesis and biological evaluation of a new series of substituted pyrrolo[2,1-*a*]isoquinolin-3-one derivatives, some of them with strong inhibitory activity against both AChE and BChE enzymes.

2. Results

2.1 Synthesis

The synthesis of compounds 1–11 has been previously reported.⁸

Four new carbamates 12–15 were synthesized by reaction between the corresponding hydroxy-pyrroloisoquinolone and the appropriate phenyl or ethyl isocyanate. 8-Phenylcarbamate-1,2,3,5,6,10*b*-hexahydropyrrolo[2,1-*a*]isoquinolin-3-one (12) was obtained from 8-hydroxy-pyrroloisoquinolinone (3), and 8-chloro-9-phenylcarbamate-1,2,3,5,6,10*b*-hexahydropyrrolo[2,1-*a*]isoquinolin-3-one (13) was prepared from 8-chloro-9-hydroxy-pyrroloisoquinolone (7). Whereas, both 8,9-bis(ethylcarbamate)- (14)



Scheme 1 Synthesis of 8-substituted and 8,9-disubstituted pyrrolo[2,1-*a*]isoquinolin-3-one derivatives. Reagents and conditions: (a) ethyl succinyl chloride, NaOH 5%, CH₂Cl₂, rt, overnight; (b) POCl₃, CH₃CN, N₂, reflux, 4 h; (c) NaBH₄; MeOH, rt, 2 h; (d) conc. HCl–EtOH (1 : 1) for 2, reflux, 3 h, or BBr₃, for 6 and 10, CH₂Cl₂, rt, 2 h; (e) ethyl or phenyl isocyanate, acetone, reflux, 3 h.

and 8,9-bis(phenylcarbamate)-1,2,3,5,6,10*b*-hexahydropyrrolo [2,1-*a*]isoquinolin-3-ones (**15**) were prepared from (\pm)-trolline (**11**) (Scheme 1).

2.2 Searching for new inhibitors of AChE

Previously, the research group of the University of Valencia reported the synthesis of compounds **1–11** (Fig. 1).⁸ Some of these compounds seemed interesting to us from a structural point of view since they resemble rivastigmine in some way (particularly compound **8**). Therefore, our first step in this study was to evaluate the inhibitory activity against AChE and BChE of these eleven compounds. These results are shown in Fig. S1–S3 (ESI[†]) and Table 1. As can be seen, none of the mono-substituted derivatives (compounds **1–4**) showed any inhibitory activity. Regarding the rest of the tested compounds, compounds **5, 6, 9–11** did not show any significant inhibitory effect. However, compounds **7** and **8** showed a strong inhibitory activity against both enzymes, AChE and BChE. This first result was quite encouraging considering that compounds **7** and **8** displayed a strong inhibitory activity. It should be noted that both compounds displayed a stronger activity against AChE than the reference compound (rivastigmine).

The lack of activity of compounds **2, 6** and **10** was not at all surprising since in both cases the presence of the benzyloxy or methoxy group in the replacement of OH has given, in general, less active compounds when these molecules and other structurally related ones have been tested against other molecular targets.^{14–16} However, for this particular series of compounds, the presence of a hydroxyl group might not be sufficient for the ligands to develop inhibitory effects. In this regard, a co-substitution of a Cl atom together with another polar moiety could be crucial since **7** and **8** displayed the lowest IC₅₀ values. In the case of compounds **1, 5** and **9**, a different behaviour is expected since these compounds are linear and such great molecular flexibility can justify their different activities. However, the dissimilar activities observed for compounds **3** and **7**

and **4** and **8** were not clear enough. In fact, at this stage of our study, we were not clear on the mechanism of action of the active compounds **7** and **8**. Thus, in order to better understand the behaviour of these new inhibitors at a molecular level, in our next step we conducted a molecular modelling study in which we paid particular attention to the molecular interactions that would stabilize the molecular complexes.

2.3 Molecular modelling

To understand more deeply our experimental results, we carried out a molecular modelling study. We conducted this study in four steps using different modelling techniques. In the first step, we conducted a docking study; in the second one, we performed simulations using molecular dynamics calculations. With these data we performed a per residue analysis and in the last step quantum mechanics calculations were made to evaluate in detail the molecular interactions that stabilize the different ligand–receptor complexes. The *Torpedo californica* AChE (TcAChE) gorge is a narrow, 20 Å long pocket composed of two binding sites for the cationic substrate acetylcholine, termed the catalytic anionic site (CAS) and the peripheral anionic site (PAS), lying at the base and entrance of the gorge, respectively.

Between the two sites, the gorge narrows due to a constriction formed by two aromatic residues, F330 and Y121 (bottle-neck region). Both CAS and PAS are lined mostly by aromatic residues that interact with the enzyme substrate ACh. When ACh or an analogue substrate like acetylthiocholine (ATCh) binds to the PAS, it forms interactions with residues Y70, Y121, W279, F330, F331 and Y334. A characteristic cation– π interaction between a quaternary amine and W279 as well as an H-bond between the acetyl moiety and Y121 are formed (PDB codes 2C4H, and 2C58). On the other hand, when ACh/ATCh binds to the CAS, a reaction occurs and the acetyl group covalently bound to catalytic serine interacts with residues from the “esteratic subsite” formed by:

(a) the catalytic triad E327, H440 and S200, (b) the backbone of residues A201, G118 and G119 that together form the “oxyanion hole” and (c) the aromatic residues W233, F288, F290 that hold the methyl group in place (PDB codes 2ACE, and 2C58). At the same time, the positively charged choline moiety interacts with CAS residues W84, Y130, E199, F330, F331, and Y442 that form the “anionic subsite”. As in the PAS, the choline quaternary amine forms a cation– π interaction with tryptophan W84. Our docking study indicates that compounds **7** and **8** are bound at the same site to that previously reported for rivastigmine (Fig. 2).¹² However, some differences might be appreciated between compounds **7** and **8**. While the spatial arrangement observed for compound **8** is very similar to that previously reported for rivastigmine,¹² compound **7** is located a little bit shifted to the bottom of the gorge (Fig. 2). In contrast, compounds **1, 5** and **9** led to a high number of possible conformations, which might be related to their lack of activity.

In turn, molecular dynamics calculations allowed us to perform a per residue analysis for these compounds. As we expected, the histogram obtained for compound **8** is closely

Table 1 Enzyme inhibition of substituted pyrrolo[2,1-*a*]isoquinolin-3-one derivatives against acetyl- and butyryl-cholinesterase. All values were expressed as IC₅₀ \pm SD, with a confidence of 95%. The IC₅₀ values were determined by regression analyses of three replicate determinations

Compound	IC ₅₀ (μ M)		SI ^b
	AChE	BChE	
1	> 50	> 50	—
2	> 50	> 50	—
3	> 50	> 50	—
4	> 50	> 50	—
5	> 50	> 50	—
6	> 50	> 50	—
7	19.25 \pm 2.88	4.26 \pm 0.78	4.52
8	11.03 \pm 0.34	1.74 \pm 0.31	6.34
9	> 50	> 50	—
10	> 50	> 50	—
11	> 50	> 50	—
Riv ^a	34.18 \pm 6.00	0.08 \pm 0.00	427.25

^a Rivastigmine (Riv) was used as a positive control. ^b SI (selectivity index) = IC₅₀ (AChE)/IC₅₀ (BChE).

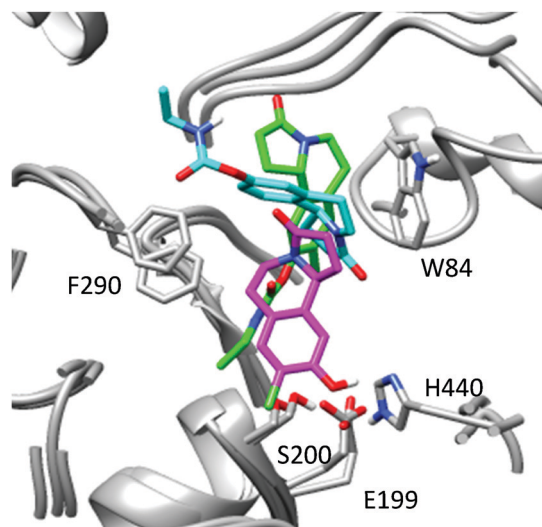


Fig. 2 Spatial view of AChE-4 (cyan), AChE-7 (magenta) and AChE-8 (green) complexes overimposed for comparison.

related to that of rivastigmine (Fig. 3A and B). The main interactions of both compounds are those with D72, W84, G118, Y121, S200, W279, F290, F330, Y334 and H440. It should be noted that the same interactions are found for compound 7. Nevertheless, interactions obtained for this compound are weaker in comparison with that observed for compound 8 (compare Fig. 3A and C). Note that compound 8 displays a stronger inhibitory activity with respect to compound 7 (Table 1); therefore, these results are in line with our experimental results. In contrast to these results, compound 4 shows a different behaviour from that observed for 8. At least two aspects show clear differences between these two compounds. One is the lack of interaction of compound 4 with S200. This can be clearly seen in the histogram obtained for this compound (Fig. 3D). It is well known that S200 plays a key role in the inhibition of AChE.^{17,18} The other important difference is that 4 adopts a completely different spatial arrangement than 7 and 8. It should be noted that compound 4 orients the pyrrole ring towards the bottom of the active site and the chain with the carbamate substituent towards the surface, in exactly the opposite form of how compound 8 is located. This can be appreciated clearly in Fig. 2.

At this stage of our study, we focused our efforts on designing and obtaining new compounds structurally related to compound 8 that possess inhibitory activity against AChE.

2.4 Design of new inhibitors of AChE and BChE

From Fig. 2 it is possible to observe that there is some room to incorporate a bulkier substituent at the carbamate group. Thus, we design four new ligands (compounds 12–15). In compounds 12 and 13 we replace the ethyl group of 4 and 8 by a phenyl group, respectively, whereas compounds 14 and 15 are the diethyl and biphenyl carbamates of compound 11. Next, we performed MD simulations for these new compounds (compounds 12–15) (Fig. 4) and the results were compared with

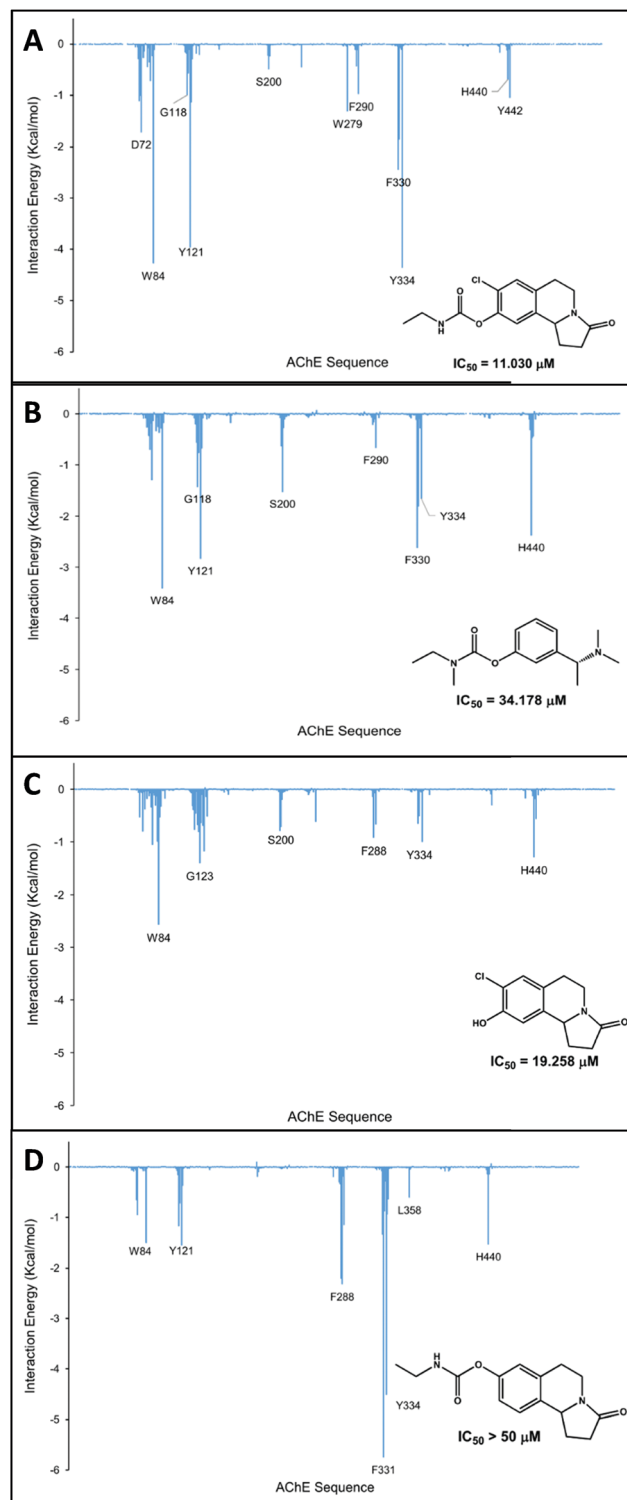


Fig. 3 Histograms of interaction energies partitioned with respect to the AChE amino acid sequence when complexed with compound 8 (A), rivastigmine (B), compound 7 (C) and compound 4 (D). The X-axis denotes the residue number of AChE and the Y-axis denotes the interaction energy between the compounds and a specific residue. Negative values and positive values are favourable or unfavourable to binding, respectively.

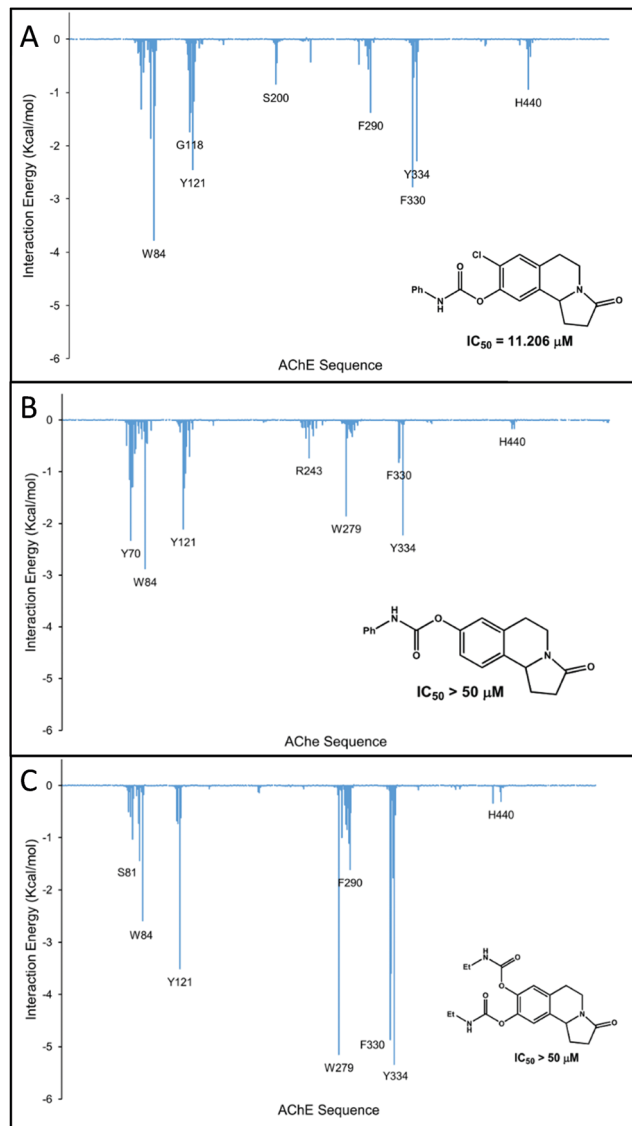


Fig. 4 Histograms of interaction energies partitioned with respect to the AChE amino acid sequence when complexed with compound **13** (A), compound **12** (B) and compound **14** (C). The X-axis denotes the residue number of AChE and the Y-axis denotes the interaction energy between the compounds and a specific residue. Negative values and positive values are favourable or unfavourable to binding, respectively.

those obtained for compounds **7** and **8**. Whereas the histogram obtained for compound **13** is closely related to that of compound **8** (compare Fig. 3A and 4A), the histograms obtained for compounds **12** and **14** (Fig. 4B and C) showed significant differences. The histogram obtained for compound **14** shows strong interactions, however the lack of interaction with S200, which is a key interaction for the inhibitory activity, is very noticeable. At the same time, those interactions with the residues from the peripheral anionic site (W279 and Y334) and from the bottleneck (F330) are clearly increased. This would be a clear indication that compound **14** could not enter into the bottom of the pocket but would remain at the surface of the active site. This different behaviour could be explained by

Table 2 Enzyme inhibition of substituted pyrrolo[2,1-a]isoquinolin-3-one derivatives against acetyl- and butyryl-cholinesterase. All values were expressed as $IC_{50} \pm SD$, with a confidence of 95%. The IC_{50} values were determined by regression analyses of three replicate determinations

Compound	IC_{50} (μM)		SI ^b
	AChE	BChE	
12	> 50	> 50	—
13	11.21 ± 1.51	14.68 ± 2.00	0.76
14	> 50	1.84 ± 0.09	—
15	> 50	> 50	—
Riv ^a	34.18 ± 6.00	0.08 ± 0.00	427.25

^a Rivastigmine (Riv) was used as a positive control. ^b SI (selectivity index) = IC_{50} (AChE)/ IC_{50} (BChE).

steric factors since compound **14** would be too bulky to enter the active site. Similar results were obtained for compound **12** (see Fig. 4B and Fig. S4, ESI[†]). The same results but even more noticeably were observed for compound **15** which is a logical result considering that the steric effects in compound **15** are stronger than those in compound **14**.

From these results, we can expect that **13** displays inhibitory effects while compounds **12**, **14** and **15** do not display or at least display a weaker activity than **13**. Thus, we decided to synthesize compounds **12–15** (see details of the synthesis in Section 2.1).

In the next step, we evaluated the inhibitory activity on both enzymes and these results are shown in Table 2. It might be seen that our experimental results are in complete agreement with the simulations, corroborating the results obtained by molecular modelling. Note that while compound **13** is one of the most active of this series, **12**, **14** and **15** showed no activity against AChE. A somewhat surprising result was that obtained for compound **14** against BChE, since although it did not show any activity on AChE, it showed a strong inhibitory activity against BChE (Table 2). To explain these results better, we performed molecular simulations for compounds **13** and **14** interacting at the active site of BChE. These results are shown in Fig. 5.

It is interesting to note that the histograms obtained for compounds **13** and **14** interacting with BChE are very similar (Fig. 5A and B) and they are closely related with that obtained for rivastigmine as well (Fig. 5C). These results indicate that in the case of BChE, compound **14** is able to enter into the bottom of the binding pocket and, therefore, it can properly interact at the CAS. Such a situation might be better appreciated in Fig. 6, which shows the spatial orderings adopted by **14** at the binding sites of both enzymes (AChE and BChE). These results might explain, at least in part, the selectivity for BChE observed in compound **14**.

Finally, considering compound **15**, our exploratory docking results showed that this ligand is too large for both active sites (AChE and BChE). The inability of compound **15** to fully enter the binding pocket does not allow the carbamate group to reach the catalytic triad. This is an expected result since changing two ethyl groups for two phenyl groups implies a considerable increase in size.

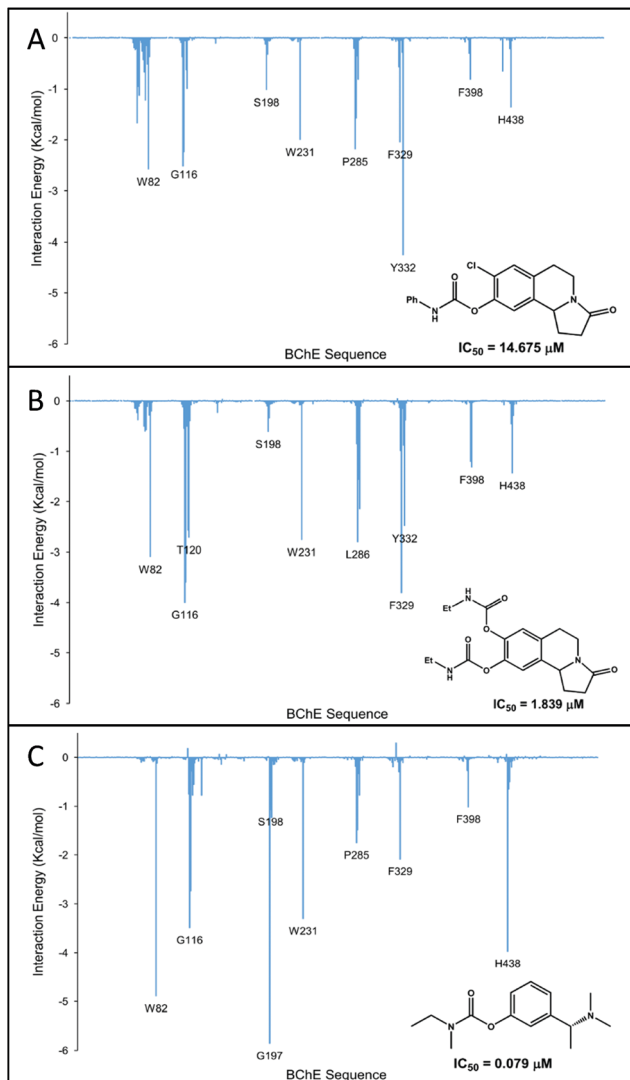


Fig. 5 Histograms of interaction energies partitioned with respect to the BChE amino acid sequence when complexed with compound **13** (A), compound **14** (B) and rivastigmine (C). The X-axis denotes the residue number of BChE and the Y-axis denotes the interaction energy between the compounds and a specific residue. Negative values and positive values are favourable or unfavourable to binding, respectively.

2.5 Molecular interactions analysis from QTAIM calculations

In a recent article, we demonstrated that QTAIM calculations are a very useful tool to evaluate in an accurate and detailed way the molecular interactions that stabilize ligand–receptor complexes possessing different degrees of structural complexity. In fact, one of the systems reported in this paper is AChE.¹⁹ On the basis of those results and with the aim of better understanding the molecular interactions involved in the different complexes reported here, we carried out a QTAIM study for the most representative ones. Thus, we selected compounds **7**, **8**, **13** and **14** complexed with AChE and compounds **13** and **14** complexed with BChE. Fig. 7 shows the binding mode of the compounds along the AChE enzyme gorge.

Upon going from A to D in Fig. 7 the ligands are more deeply buried in the gorge. Compound **14** has two bulky *N*-ethyl carbamate groups attached to the tricyclic core that prevent it from accessing the CAS through the bottleneck. When one of the bulky carbamate groups in **14** is replaced by chlorine, as in compound **8**, entrance to the CAS through the bottleneck is allowed. However, compound **8** does not completely enter the CAS but it remains halfway between both gorge sites.

According to a previous study describing TcAChE substrate trafficking, the substrate analog ACh first binds to the PAS with the acetyl group oriented towards the active site and the quaternary amine forming a cation– π interaction with the W279 ring. The observed orientation allows the substrate to slide straight through the gorge without the necessity of reorienting before productive interaction at the active site, as the CH₃CO group needs to approach the catalytic serine. In this sense, binding at the PAS may serve as a “filter” that orients the ACh molecule before it continues its journey towards the CAS.²⁰ Analogously, in complexes of compounds **14** and **8** the carbamate moiety is also pointing down towards the active site while the electropositive amide from the γ -lactam ring is stacked over the W279 ring (Fig. 7A and B).

On the other hand, the binding of compound **13** to the CAS also closely resembles that of the substrate: the carbonyl oxygen atom points toward the oxyanion hole (*i.e.* the backbone of S200 and A201 in Fig. 7) and the activated carbon atom is properly positioned for nucleophilic attack by S200 (PDB code 2ACE). Furthermore, the electron-deficient γ -lactam ring of compound **13** is stacked on top of W84 in the same way as the substrate quaternary amine is also stacked over the same ring through a cation– π interaction.

One of the most salient characteristics of these carbamate derivatives is the overall curved shape provided by the tricyclic core, which allows a good fit of these compounds within the CAS. Potent carbamate inhibitor physostigmine also has a similar curved tricyclic core and its binding mode resembles that of compound **13** where the curved ring of the molecule is lying on top of the W84 indole ring.²¹ Therefore, agreement between our structural models and previous structural evidence of substrate analogue binding to both the CAS and the PAS enable us to be confident in the reliability of our computational predictions, at least from a qualitative point of view.

2.5.1 Charge density analysis of molecular interactions.

Regarding the stability of the structural models, the stacked bars in Fig. 8 provide a dissected view of the anchoring of carbamate compounds to the different sites within the TcAChE gorge.

As indicated by the stacked bars in Fig. 8, compound **14** binds almost completely to the PAS, compounds **7** and **13** are mostly anchored to the CAS, whereas compound **8** is in between both sites. An unexpected result revealed by the charge density data in Fig. 8 is that anchoring to the PAS is actually stronger than to the CAS, as indicated by the contribution of the PAS residues to the overall anchoring of compounds **14** and **8** (*i.e.* yellow stacked bars). Nevertheless, the activity of these carbamates seems to be conditioned to their ability to reach the

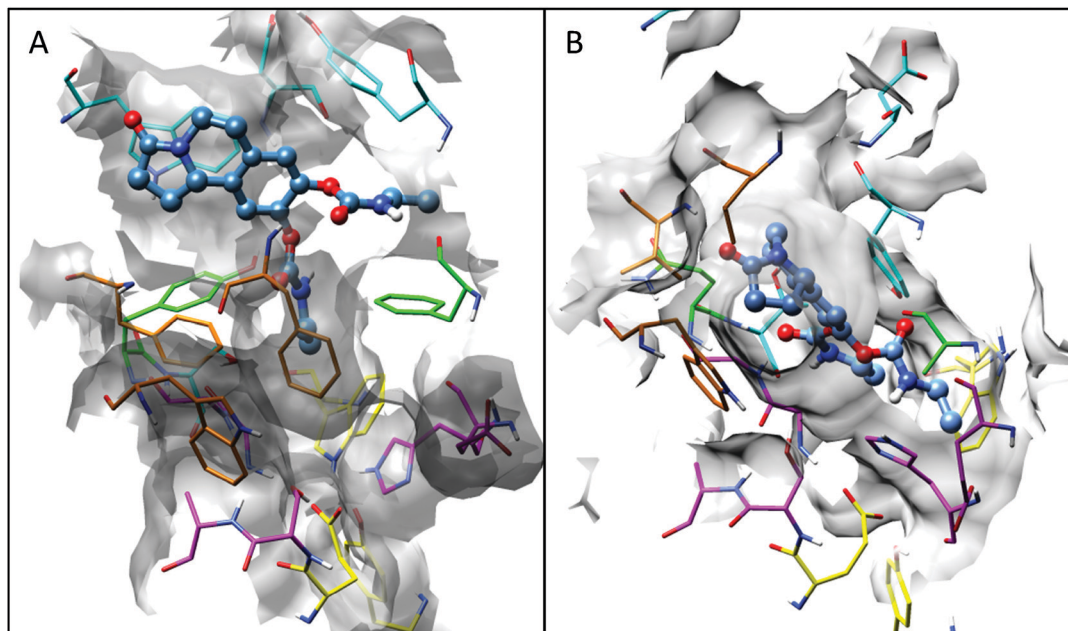


Fig. 6 Active sites of *Torpedo californica* AChE (A) and *Homo sapiens* BChE (B) when complexed with compound **14**, which is represented in ball-and-stick format and coloured in blue. The gorge of each enzyme is depicted by its molecular surface in semi-transparent grey. The main amino acid residues from both active sites are also shown. Residues from the CAS including the catalytic triad and oxyanionic subsite are depicted in magenta. Amino acids from the acyl-binding pocket and the anionic subsite are represented in orange and yellow, respectively. Residues from the PAS and the bottleneck region are depicted cyan and green, respectively.

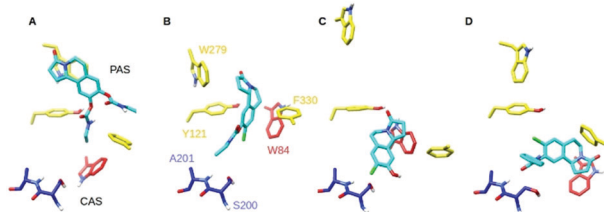


Fig. 7 Binding modes of compounds **14** (A), **8** (B), **7** (C) and **13** (D) within the TcAChE gorge. Residues from the CAS-esteratic, CAS-anionic and PAS are depicted in blue, red and yellow, respectively. In order to reach the CAS at the bottom of the gorge, the ligand must slide through the bottleneck formed by side-chains of residues Y121 and F330.

CAS regardless of its anchoring strength and, so, compound **14** is inactive since it is not able to enter the CAS. Exclusive binding to the PAS is only observed when high concentrations of the substrate analogue are present in the crystallization solution, suggesting that the PAS is occupied only transiently,²⁰ which is also reflected in the very high IC_{50} value reported for the binding of compound **14** at the TcAChE gorge.

On the other hand, compound **8** seems to benefit from anchoring at both sites simultaneously. It is likely that compound **8** was captured in a transient intermediate state along the way to the enzyme active site at the bottom of the gorge. Unlike compound **14**, there is no reason why **8** could not reach the gorge base since it is even less bulky than compound **13** (Fig. 7). However, because of the stronger interactions with the PAS residues, anchoring at this intermediate state (*i.e.* in between both sites) is stronger than binding at the bottom of the gorge (compare the stacked bars for **8** and **13** in Fig. 8).

Known AChE inhibitors like potent donepezil and galantamine also target both the PAS and CAS simultaneously (PDB entries 4EY7, 1EVE and 1W6R, 4EY6, respectively).

Charge density molecular graphs in Fig. 9 and 10 show in more detail the molecular interactions that contribute to the anchoring of compounds **13** and **8**, respectively.

Compound **13** mainly interacts with residues from the CAS at the gorge base and the carbamoyl group is well positioned within the esteratic subsite for nucleophilic attack by the reactive serine residue. Fig. 9 shows that the carbamoyl oxygen atom is hydrogen bonded to the oxyanion hole as evidenced by the bond paths connecting this atom to backbone H atoms from A201, G117 and G119, thus enhancing the electrophilicity of the carbamoyl carbon atom so that it might then be eventually attacked by the reactive S200 oxygen atom.

Also, several C–H $\cdots\pi$ interactions between the *N*-phenyl group and ring atoms from aromatic residues W233, F288 and F290 contribute to binding of the carbamoyl moiety at the esteratic subsite. Moreover, the terminal γ -lactam ring from the tricyclic core is stacked over W84, forming several C–H $\cdots\pi$ interactions between them that together make an important contribution to the anchoring of compound **8** (see Fig. 7).

On the other hand, as compound **8** has not fully accessed the CAS the carbamoyl group is too far from the reactive S200 and it is not properly oriented within the oxyanion hole (Fig. 10). Misplacement of the carbamoyl group is reflected in the overall weaker binding to the esteratic subsite compared with compound **13** (see Fig. 7). However, interactions of the tricyclic core structure with aromatic residues from the PAS compensate for the anchoring loss from the CAS and so the

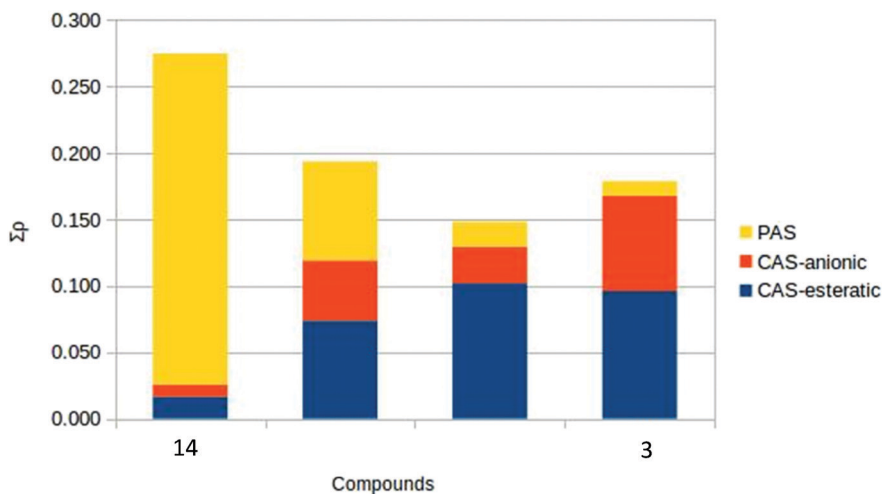


Fig. 8 Sum of charge density values (in atomic units) at the intermolecular bond critical points between TcAChE and the selected compounds. The total height of stacked bars indicates the overall anchoring strength of the compounds within the gorge which can be decomposed into anchoring to the CAS esteratic subsite (CAS-esteratic), CAS anionic subsite (CAS-anionic) and PAS site.

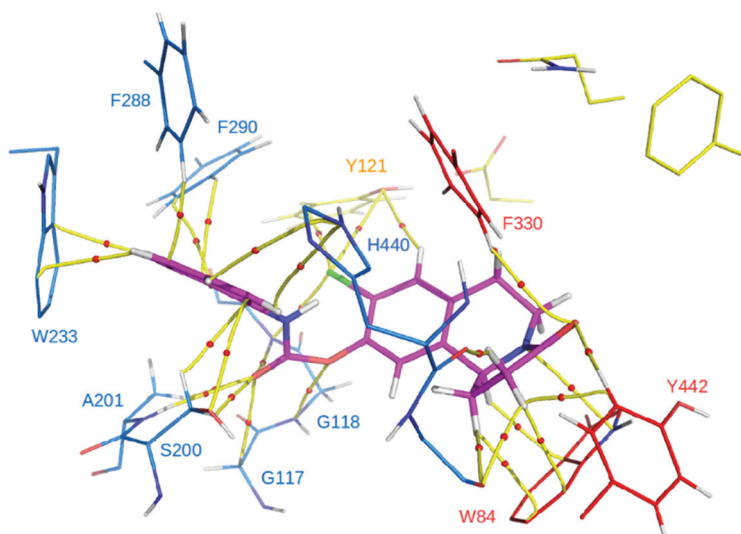


Fig. 9 Charge density molecular graph of compound **13** (magenta) at the gorge of TcAChE. Residues from the CAS-esteratic, CAS-anionic and PAS are depicted in blue, red and yellow, respectively. Topological elements of the charge density associated with the intermolecular interactions are depicted with yellow lines (Bond Paths, BPs) and small red spheres (Bond Critical Points, BCPs).

overall binding of compound **8** ends up being stronger than for compound **13**.

Moreover, although the overall structures of BChE and AChE are similar, their interactions with the same ligands are generally different due to slight differences in their residue sequences. Bottleneck aromatic residues F330 and Y121 that separate the PAS from the CAS in AChE are replaced in BChE by the less bulky A328 and Q119, respectively. As a result, there is no longer such a bottleneck between the PAS and CAS in BChE, such that ligands that could not access the CAS in AChE due to their size might now be able to do so in BChE. This seems to be the case for bulky compound **14**, as indicated by the interaction profile in Fig. 5B which resembles that of rivastigmine (Fig. 5C).

Fig. 11 shows in more detail the interactions of compound **14** at the BChE gorge.

As can be seen in Fig. 11, compound **14** is certainly anchored at the bottom of the gorge between aromatic residues W82 and W231 that make up the walls of the CAS at both ends of its longer (longitudinal) axis. However, unlike rivastigmine that bind its carbamate moiety to the esteratic subsite, our modelling results suggest that compound **14** binds in the opposite way, namely with the carbamate moiety placed at the CAS-anionic subsite. The fact the compound **14** can bind to the CAS of BChE, albeit not in the expected orientation, correlates well with the inhibition data, namely that it is able to inhibit BChE but with much less potency than rivastigmine.

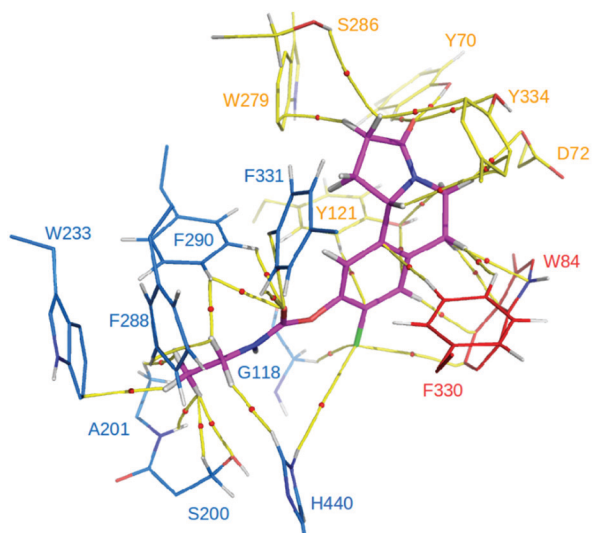


Fig. 10 Charge density molecular graph of compound **8** (magenta) at the gorge of TcAChE. Residues from the CAS-esteratic, CAS-anionic and PAS are depicted in blue, red and yellow, respectively. Topological elements of the charge density associated with the intermolecular interactions are depicted with yellow lines (Bond Paths, BPs) and small red spheres (Bond Critical Points, BCPs).

To understand the origin of the binding mode differences of the compounds to BChE and AChE, Fig. 11 and 12 shows key active site residues from TcAChE that are mutated in HsBChE. In particular, Fig. 11 shows residues W279 and Y121 from the TcAChE structure (in grey) that have been previously superposed with the HsBChE structure. These residues form a specialized structure at the PAS of TcAChE in which Y121 is held firmly on top of the CAS by T-shaped C-H \cdots π interactions

with W279. In this arrangement, Y121 partially covers the CAS entrance as can be seen in Fig. 11. In BChE, both residues W279 and Y121 are replaced by A277 and Q119 respectively, so that they are no longer able to interact with each other and consequently Q119 is displaced away from the CAS entrance. Because of these substitutions (as well as the substitution of F330 by A328), larger ligands can access the bottom of the gorge in HsBChE, as compared with TcAChE.

Besides the role of the specialized structure formed by residues W279 and Y121 as a ligand size-based filter, these residues at the PAS of TcAChE are also involved in ligand pre-orientation by accommodating the hydrolysable tail (*i.e.* the carbamate moiety) in such a way that it can slide straight through the CAS-esteratic subsite, as already discussed previously. Thus, the lack of a pre-orientational filter at the PAS of BChE might be allowing the inverted binding mode of compound **14** at the CAS of the enzyme.

Fig. 12 shows the interactions of compound **13** as it binds to the HsBChE gorge. The binding mode of compound **13** to TcAChE is also shown in grey for comparison. As can be seen in Fig. 12, compound **13** is anchored at the CAS of both TcAChE and HsBChE; however, it is able to reach the bottom of the gorge base only in the first case. This difference is likely due to the substitution of residue V400 in TcAChE (in grey in Fig. 12) by the bulkier F398 in HsBChE, which prevents the *N*-phenyl carbamate moiety of compound **13** from fully accessing the CAS-esteratic subsite. As a consequence, the hydrolysable carbamate moiety of compound **13** is not properly placed for nucleophilic attack by the reactive serine in HsBChE, as it does in TcAChE. These modelling results are also in line with the inhibition data, which show that compound **13** is a slightly more potent inhibitor of TcAChE than HsBChE.

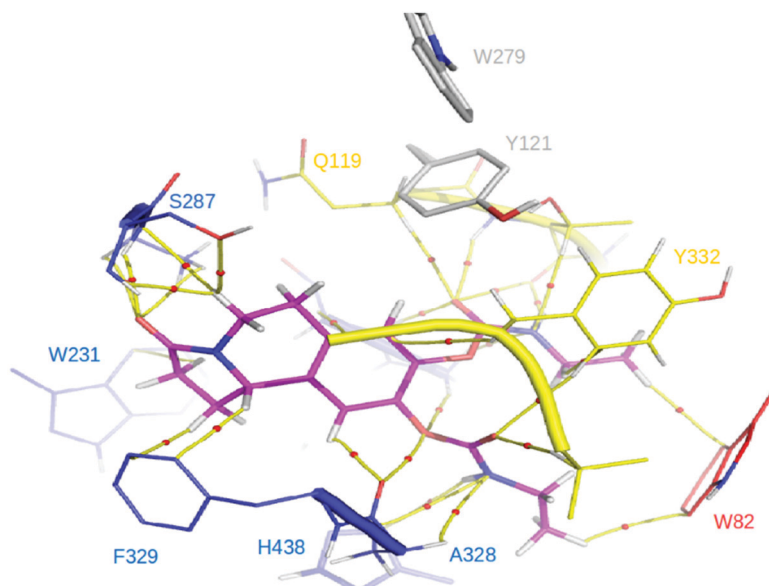


Fig. 11 Charge density molecular graph of compound **14** (magenta) at the gorge of HsBChE. Residues from the CAS-esteratic, CAS-anionic and PAS are depicted in blue, red and yellow, respectively. Residues in grey are not from BChE structure but from a superimposed TcAChE structure. Topological elements of the charge density associated with the intermolecular interactions are depicted with yellow lines (Bond Paths, BPs) and small red spheres (Bond Critical Points, BCPs).

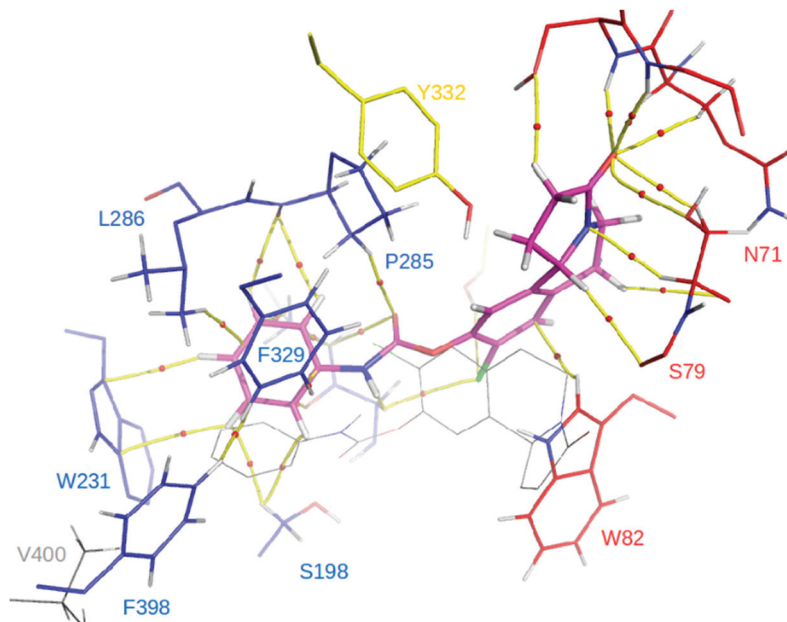


Fig. 12 Charge density molecular graph of compound **13** (magenta) at the gorge of HsBChE. Residues from the CAS-esteratic, CAS-anionic and PAS are depicted in blue, red and yellow, respectively. The binding mode of compound **13** to TcAChE as well as residue V400 from TcAChE have been superimposed for comparison (in grey). Topological elements of the charge density associated with the intermolecular interactions are depicted with yellow lines (Bond Paths, BPs) and small red spheres (Bond Critical Points, BCPs).

Although the results obtained from molecular modelling simulations represent additional support for the possible effect on AChE and BChE, further studies, as for example a kinetic analysis, could give a better and more complete understanding about the inhibitory effect displayed by these compounds.

3. Methodology

3.1 General experimental procedures and instrumentation

All solvents and reagents were purchased from Scharlab S.L. (Barcelona, Spain) and Sigma-Aldrich (St Louis, MO) commercial sources. Solvents were dried and freshly distilled under a nitrogen atmosphere if necessary. ^1H and ^{13}C NMR spectra were recorded using CDCl_3 as the reference solvent with two drops of CD_3OD if necessary in a Bruker AC-300 or AC-500 spectrometer (Bruker Instruments, Kennewick, WA). Chemical shifts (δ) are reported in ppm relative to an internal deuterated solvent reference. Multiplicities of the ^{13}C NMR resonances were assigned by DEPT experiments. The assignments of all compounds were made by COSY, DEPT, HSQC and HMBC. All reactions were monitored by analytical thin-layer chromatography (TLC), carried out on silica gel 60 F254 plates (Merck Group, Darmstadt, Germany), and visualized by UV irradiation at 254 nm. ESIMS analyses were performed using UHPLC apparatus (Shimadzu, LCMS-8040) coupled to a tandem mass spectrometry (MS/MS) triple quadrupole instrument equipped with an electrospray ionization (ESI) ion source (Shimadzu, Kyoto, Japan). High-resolution electron ionization mass spectrometry (HREIMS) was determined by a TripleTOF 5600 LC/MS/MS system (AB SCIEX, Framingham, MA, U.S.A.). Residues

were purified by silica gel 60 (40–63 μm , Merck) column chromatography. The quoted yields are of the purified material.

3.2 Synthesis

3.2.1 Synthesis of 8,9-disubstituted pyrrolo[2,1-*a*]isoquinolinone derivatives. The general synthetic path for compounds **1–11** has been previously reported. 8-Substituted (**12**) and 8,9-disubstituted (**13–15**) pyrrolo[2,1-*a*]isoquinolinone carbamate derivatives were prepared according to ref. 8.

3.2.2 General procedure for the synthesis of carbamate derivatives (8, 12–15)

*8-Hydroxy-1,2,3,5,6,10b-hexahydropyrrolo[2,1-*a*]isoquinolin-3-one (3).* 8-Chloro-9-hydroxy-1,2,3,5,6,10b-hexahydropyrrolo[2,1-*a*]isoquinolin-3-one (**7**) or 8,9-dihydroxy-1,2,3,5,6,10b-hexahydropyrrolo[2,1-*a*]isoquinolin-3-one (**11**) (1 equiv.) was dissolved in dry acetone (10 mL). Subsequently, the appropriate ethyl or phenyl isocyanate (1.5 equiv. or 3 equiv. for **12**, **13** or **14**, **15** respectively) was added. The reaction mixture was heated under reflux for 3 h and then concentrated to dryness. The residue was redissolved in 10 mL of CH_2Cl_2 and washed with H_2O (3×10 mL). The organic layer was dried with anhydrous Na_2SO_4 , filtered and evaporated under reduced pressure. The crude product was purified by column chromatography on silica gel ($\text{CH}_2\text{Cl}_2/\text{MeOH}$ 97 : 3).

*8-Phenylcarbamate-1,2,3,5,6,10b-hexahydropyrrolo[2,1-*a*]isoquinoline-3-one (12).* Colourless oil (13 mg, 27% yield). ^1H NMR (300 MHz, CDCl_3): δ = 7.44 (2H, d, J = 8.0 Hz, H-2', H-6'), 7.34 (1H, t, J = 7.4 Hz, H-4'), 7.16–7.08 (2H, m, H-3', H-5'), 6.97 (1H, d, J = 8.4 Hz, H-10), 6.75 (1H, dd, J = 2.6, 8.4 Hz, H-9), 6.63 (1H, d, J = 2.6 Hz, H-7), 6.20 (1H, brs, NH), 4.78–4.69

(1H, m, H-10b), 4.32–4.21 (1H, m, Ha-5), 3.11–2.47 (6H, m, Hb-5, H-6, Ha-1, H-2), 1.92–1.80 (1H, m, Hb-1); ^{13}C NMR (75 MHz, CDCl_3): δ = 173.1 (CO-3), 154.8 (NHCO), 149.1 (C-8), 137.2 (C-1'), 135.1 (C-6a), 129.4 (C-10a), 129.2 (CH-4'), 126.0 (CH-10), 125.9 (CH-3', CH-5'), 119.0 (CH-2', CH-6'), 115.3 (CH-7), 114.3 (CH-9), 56.5 (CH-10b), 37.0 (CH2-5), 31.8 (CH2-2), 28.6 (CH2-6), 27.7 (CH2-1); HREIMS: m/z 322.1374 $[\text{M}]^+$ (calcd for $\text{C}_{19}\text{H}_{18}\text{N}_2\text{O}_3$, 322.1310).

8-Chloro-9-phenylcarbamate-1,2,3,5,6,10b-hexahydropyrrolo[2,1-a]isoquinoline-3-one (13). Colourless oil (7.5 mg, 25% yield). ^1H NMR (500 MHz, CDCl_3): δ = 7.46 (2H, d, J = 8.0 Hz, H-2', H-6'), 7.35 (1H, t, J = 7.4 Hz, H-4'), 7.26 (1H, s, H-7), 7.17–7.12 (2H, m, H-3', H-5'), 7.03 (1H, s, H-10), 4.75 (1H, t, J = 7.8 Hz, H-10b), 4.30 (1H, ddd, J = 2.6, 6.2, 12.9 Hz, Ha-5), 3.08–3.01 (1H, m, Hb-5), 2.95–2.87 (1H, m, Ha-6), 2.80–2.75 (1H, m, Hb-6), 2.67–2.62 (1H, m, Ha-1), 2.61–2.55 (1H, m, Ha-2), 2.51–2.45 (1H, m, Hb-2), 1.90–1.86 (1H, m, Hb-1); ^{13}C NMR (125 MHz, CDCl_3): δ = 173.1 (CO-3), 150.5 (NHCO), 145.3 (C-9), 137.3 (C-10a), 137.0 (C-1'), 132.8 (C-6a), 130.6 (CH-7), 129.2 (CH-4'), 125.7 (CH-3', CH-5'), 124.2 (C-8), 120.4 (CH-10), 118.7 (CH-2', CH-6'), 56.3 (CH-10b), 36.7 (CH2-5), 31.6 (CH2-2), 27.9 (CH2-6), 27.2 (CH2-1); HREIMS: m/z 357.1011 $[\text{M}]^+$ (calcd for $\text{C}_{19}\text{H}_{17}\text{ClN}_2\text{O}_3$, 357.1000).

8,9-Bis(ethylcarbamate)-1,2,3,5,6,10b-hexahydropyrrolo[2,1-a]isoquinoline-3-one (14). Colourless oil (12 mg, 36% yield). ^1H NMR (300 MHz, CDCl_3 + 2 drops CD_3OD): δ = 6.97 (1H, s, H-10), 6.95 (1H, s, H-7), 5.21–5.17 (2H, m, NH), 4.71 (1H, t, J = 6.7 Hz, H-10b), 4.25 (1H, ddd, J = 12.7, 6.0, 2.8 Hz, Ha-5), 3.34–3.24 (4H, m, CH₂NH), 3.03 (1H, td, J = 1.0, 4.2 Hz, Hb-5), 2.95–2.80 (1H, m, Ha-6), 2.78–2.67 (1H, m, Hb-6), 2.65–2.40 (3H, m, Ha-1, H-2), 1.95–1.80 (1H, m, Hb-1), 1.19 (3H, t, J = 7.0 Hz, CH₃CH₂NH); ^{13}C NMR (75 MHz, CDCl_3 + 2 drops CD_3OD): δ = 173.7 (CO-3), 157.8 (NHCO), 141.7 (C-9), 141.5 (C-8), 135.1 (C-10a), 131.5 (C-6a), 123.6 (CH-10), 119.7 (CH-7), 56.5 (CH-10b), 36.8 (CH2-5), 35.9 (CH₂NH), 31.5 (CH2-2), 27.8 (CH2-6), 27.0 (CH2-1), 14.7 (CH₃CH₂NH); HREIMS: m/z 362.1714 $[\text{M}]^+$ (calcd for $\text{C}_{18}\text{H}_{23}\text{N}_3\text{O}_5$, 362.1710).

8,9-Bis(phenylcarbamate)-1,2,3,5,6,10b-hexahydropyrrolo[2,1-a]isoquinoline-3-one (15). Colourless oil (15 mg, 41% yield). ^1H NMR (300 MHz, CDCl_3): δ = 7.41–7.03 (10H, m, 2xH-2', 2xH-3', 2xH-4', 2xH-5', 2xH-6'), 7.12–7.06 (1H, s, H-10), 7.03 (1H, s, H-7), 4.79–4.66 (1H, m, H-10b), 4.27–4.15 (1H, m, Ha-5), 3.07–2.82 (2H, m, Hb-5, Ha-6), 2.81–2.69 (1H, m, Hb-6), 2.68–2.41 (3H, m, Ha-1, H-2), 1.98–1.76 (1H, m, Hb-1); ^{13}C NMR (75 MHz, CDCl_3): δ = 173.3 (CO-3), 150.8 (NHCO), 141.2, 140.9 (C-8, C-9), 136.4 (C-1'), 136.0 (C-6a), 132.3 (C-10a), 129.2 (CH-4'), 124.5 (CH-10), 124.0 (CH-3', CH-5'), 120.1 (CH-7), 118.7 (CH-2', CH-6'), 56.4 (CH-10b), 36.8 (CH2-5), 31.6 (CH2-2), 28.1 (CH2-6), 27.1 (CH2-1); HREIMS: m/z 475.1977 $[\text{M} + \text{H}_2\text{O}]^+$ (calcd for $\text{C}_{26}\text{H}_{23}\text{N}_3\text{O}_5$, 475.1976).

3.3 AChE and BChE inhibitory activity

End-point inhibitory activity was tested according to a previously reported method.²² For each sample, an Ellman's reaction²³ was performed in a final volume of 200 μL with

0.25 U mL^{-1} of EeAChE (E.C. 3.1.1.7, type VI-S from the electric eel, Sigma-Aldrich), 0.24 mM of acetylthiocholine (ATCh), 0.2 mM of DTNB and the corresponding compound (50–3.125 μM). The reaction started after the addition of the substrate to a 15 min pre-incubated solution of AChE with the compound. Absorbance at 405 nm was measured after 5 min using a 96-well microplate reader (Thermo Fisher FC Multiskan). The AChE inhibition percentage ($I\%$) was calculated with eqn (1). Each compound was tested in triplicate. The AChE residual activity percentage (equal to $100 - I\%$) values were used to calculate the required concentration to inhibit 50% of enzyme activity (IC_{50}) with a four-parameter logistic curve.

$$\% I = (\text{AI} - \text{Ab}) \times 100 / (\text{A0} - \text{Ab}) \quad (1)$$

A0: control (no inhibitor); Ab: blank (no enzyme, no inhibitor); AI: sample.

The same procedure was applied for the BChE inhibitory assay, with modifications in the enzyme and substrate used, which were BChE from human serum and *S*-butyrylthiocholine iodide (BTCI; 7 mM), respectively.

In both cases, rivastigmine was used as a positive control.

3.4 Molecular modelling

Calculations were performed after synthesizing previously reported compounds 1–11. Conversely, all simulations regarding new derivatives 12–15 were conducted before their synthesis.

3.4.1 Molecular docking. The following X-ray structures available in the Protein Data Bank (<http://www.rcsb.org>) were used for molecular modelling studies: *Torpedo californica* acetylcholinesterase (TcAChE; PDB code: 1DX6)²⁴ and *Homo sapiens* butyrylcholinesterase (HsBChE; PDB code: 6EUL).²⁵ Water and ligand molecules were removed from both PDB structures before calculations. Compounds 1–15 and receptor structures were converted from PDB to PDBQT format using AutoDockTools 1.5.4.²⁶ Gasteiger charges were added for all the compounds whereas non-polar hydrogen atoms were merged. The docking simulations were performed using AutoDock 4.2 software.²⁶ In all simulations, the receptor structure was set as rigid while all the torsions of the ligand were allowed to rotate during docking. 3D affinity maps were defined as a cubic box centred at the active site of each molecular target. Grid dimensions (XYZ) were 60 \times 60 \times 60 points separated by 0.375 Å. The maximum number of energy evaluations was set to 2.5×10^6 , and the maximum number of generations was 2.7×10^4 whereas 200 poses were collected. Other parameters were set to default values. The collected conformations were clustered into different families, taking into account the root-mean square deviation (RMSD) of the backbone, and were then ranked according to the binding free energy. The structure from the most populated cluster with the lower relative free energy was chosen for further calculations.

3.4.2 Molecular dynamics (MD). MD simulations of all complexes and later analysis of their trajectories were performed with the Amber16 package.²⁷ Antechamber software

in the AmberTools package²⁸ was used to generate the parameters for MD simulations with ff99SB²⁹ and GAFF³⁰ force fields. The best ranked conformation of each complex was then soaked in truncated octahedral periodic boxes of explicit water boxes using the TIP3P model.³¹ Na⁺ or Cl⁻ ions were placed using the Leap module to neutralize the negative and positive charges of the AChE and BChE complexes, respectively. The energy of each system was minimized with the sander module using a steepest-descent algorithm for 1000 steps. Subsequently, the complexes were equilibrated during 500 ps at constant volume. The SHAKE algorithm³² was applied allowing for an integration time step of 2 fs. The systems were heated up to 300 K, a Langevin thermostat³³ was applied and the collision frequency was 1.0 ps⁻¹. After minimization and heating, three MD production simulations of 20 ns were carried out at a 298 K target temperature. Thus, in total 60 ns were simulated for each complex. Coordinates were saved for analysis every 10 ps. All productions were performed under *NVT* conditions and the particle mesh Ewald method (PME)³⁴ was applied using a grid spacing of 1.2 Å, a spline interpolation order of 4 and a real space direct sum cutoff of 10 Å. Post MD analysis was performed with the program CPPTRAJ.³⁵

3.4.3 MM-PBSA free energy calculation and per-residue analysis. MMPBSA calculations were conducted to calculate the relative binding energies of the complexes.³⁶ Snapshots from the corresponding last 1000 ps of the MD trajectories were considered. The explicit water molecules and counter ions were removed from the snapshots.

Afterwards, a per-residue decomposition of the relative free energy was performed using the *mm_pbsa* program in the AMBER package. This analysis led us to determine which amino acids of the AChE and BChE catalytic sites are involved in the interactions with each ligand.

3.4.4 Quantum mechanics calculations and topological analysis of the electron density distribution. MD trajectories were first clustered based on the root mean square deviation (RMSD) of the complex backbone atoms employing the CPPTRAJ tool included in the Amber package. Then, the representative structure from the most populated clusters was selected for the QTAIM analysis.

Reduced 3D model systems representing the different L-R binding pockets of the selected zones were constructed from the representative structures obtained by MD simulations by keeping only receptor residues that interact directly with the ligands. All the amino acids that are within a radius of 5 Å distance from each ligand atom were considered. Those residues that showed significant interactions with the ligand in the free energy decomposition approach were also included.

The charge density of the reduced model systems was then computed by DFT methodology with the PBE hybrid functional and the 6-31G(d) as basis set, as implemented in the Gaussian 16 package.³⁷ The topological analysis of charge density was performed on the different reduced models to evaluate the interactions between each ligand and the molecular target in the context of the quantum theory of atoms in molecules (QTAIM).³⁸ These calculations were carried out with the help

of the Multiwfn software.³⁹ This type of calculation has been used in recent works since it ensures a reasonable compromise between the wave function quality required to obtain reliable values of the derivatives of $\rho(r)$ and the computer power available.^{12,19,40-45}

4. Conclusions

We report here a new series of inhibitors of AChE and BChE. Some of the substituted pyrrolo[2,1-*a*]isoquinolinone derivatives reported here exhibit a significant inhibitory effect against both the AChE and BChE enzymes. Among the series reported here, compounds **7**, **8**, **13** and **14** were those that displayed more strong inhibitory activities; most of them possessed inhibitory effects even stronger than rivastigmine (the compound used as the reference). It should be noted that compound **14** was the only one showing a selective inhibitory activity against BChE. The molecular modelling study showed that the larger size of the active site of BChE with respect to AChE could explain the selective activity of compound **14**. QTAIM analysis gave us detailed information about the molecular interactions stabilizing the different ligand-enzyme complexes. Such information could be useful for the study and design of new inhibitors of both enzymes.

Author contributions

O. P. and R. D. E. contributed to the conceptualization of this work. O. P., L. V., N. C. and D. C. carried out the synthesis and characterization of the compounds. O. P. and F. G. performed the molecular modelling studies. O. P., E. A. and R. D. E. conducted the QTAIM calculations. R. S. and A. S. S. carried out the bioassays studies and their analysis. O. P., E. A., N. C., D. C. and R. D. E. wrote and corrected the article.

Conflicts of interest

There are not conflicts to declare.

Acknowledgements

The manuscript was written through contributions of all authors. The continued funding of the UNSL is strongly appreciated. This work has also been partially funded by grants from ANPCyT (PICT 2015-1769). This study was also supported by grants from the Spanish Ministry of Economy and Competitiveness (SAF2017-89714-R) and the Carlos III Health Institute (PI18/01450) and the European Regional Development Fund. NC is an investigator from the "Miguel Servet" programme (CP15/00150), from Carlos III Institute of Health, co-funded by the European Social Fund. RDE, FG, EA, RS and AS are members of CIC-CONICET-ARGENTINA.

References

- 1 M. Prince, A. Comas-Herrera, M. Knapp, M. Guerchet and M. Karagiannidou, World Alzheimer Report 2016 Improving healthcare for people living with dementia coverage, Quality and costs now and In the future.
- 2 H. Brodaty and M. Donkin, *Dialogues Clin. Neurosci.*, 2009, **11**, 217–228.
- 3 M. Ma, D. Dorstyn, L. Ward and S. Prentice, *Aging Ment. Heal.*, 2018, **22**, 1395–1405.
- 4 L. Patel and G. T. Grossberg, *Drugs Aging*, 2011, **28**, 539–546.
- 5 P. Taylor, in *The Pharmacological Basis of Therapeutics*, ed. A. Gilman, A. Nies, T. Rall and P. Taylor, MacMillan, New York, United States, 5th edn, 1990, pp. 131–150.
- 6 D. M. Bowen, C. B. Smith, P. White and A. N. Davison, *Brain*, 1976, **99**, 459–496.
- 7 P. Davies, *Brain Res.*, 1979, **171**, 319–327.
- 8 L. Moreno, J. Parraga, A. Galan, N. Cabedo, J. Primo and D. Cortes, *Bioorg. Med. Chem.*, 2012, **20**, 6589–6597.
- 9 F. Carmona-Viglianco, D. Zaragoza-Puchol, O. Parravicini, A. Garro, R. D. Enriz, G. E. Feresin, M. Kurina-Sanz and A. A. Orden, *New J. Chem.*, 2020, **44**, 9466–9476.
- 10 A. Hudcová, A. Kroutil, R. Kubínová, A. D. Garro, L. J. Gutierrez, D. Enriz, M. Oravec and J. Csöllei, *Molecules*, 2020, **25**, 1751.
- 11 J. E. Ortiz, A. Garro, N. B. Pigni, M. B. Agüero, G. Roitman, A. Slanis, R. D. Enriz, G. E. Feresin, J. Bastida and A. Tapia, *Phytomedicine*, 2018, **39**, 66–74.
- 12 T. Padrtova, P. Marvanova, K. Odehnalova, R. Kubinova, O. Parravicini, A. Garro, R. Enriz, O. Humpa, M. Oravec and P. Mokry, *Molecules*, 2017, **22**, 2048.
- 13 J. E. Ortiz, N. B. Pigni, S. A. Andujar, G. Roitman, F. D. Suvire, R. D. Enriz, A. Tapia, J. Bastida and G. E. Feresin, *J. Nat. Prod.*, 2016, **79**, 1241–1248.
- 14 J. Parraga, S. A. Andujar, S. Rojas, L. J. Gutierrez, N. El Aouad, M. J. Sanz, R. D. Enriz, N. Cabedo and D. Cortes, *Eur. J. Med. Chem.*, 2016, **122**, 27–42.
- 15 O. Parravicini, M. L. Bogado, S. Rojas, E. L. Angelina, S. A. Andujar, L. J. Gutierrez, N. Cabedo, M. J. Sanz, M. P. López-Gresa, D. Cortes and R. D. Enriz, *J. Mol. Model.*, 2017, **23**, 273.
- 16 J. Parraga, N. Cabedo, S. Andujar, L. Piqueras, L. Moreno, A. Galan, E. Angelina, R. D. Enriz, M. D. Ivorra, M. J. Sanz and D. Cortes, *Eur. J. Med. Chem.*, 2013, **68**, 150–166.
- 17 P. Bar-On, C. B. Millard, M. Harel, H. Dvir, A. Enz, J. L. Sussman and I. Silman, *Biochemistry*, 2002, **41**, 3555–3564.
- 18 M. B. Colovic, D. Z. Krstic, T. D. Lazarevic-Pasti, A. M. Bondzic and V. M. Vasic, *Curr. Neuropharmacol.*, 2013, **11**(3), 315–335.
- 19 S. Rojas, O. Parravicini, M. Vettorazzi, R. Tosso, A. Garro, L. Gutiérrez, S. Andújar and R. Enriz, *Eur. J. Med. Chem.*, 2020, **208**, 112792.
- 20 J.-P. Colletier, D. Fournier, H. M. Greenblatt, J. Stojan, J. L. Sussman, G. Zaccai, I. Silman and M. Weik, *EMBO J.*, 2006, **25**, 2746–2756.
- 21 D. Barak, A. Ordentlich, D. Stein, Q. S. Yu, N. H. Greig and A. Shafferman, *Biochem. J.*, 2009, **417**, 213–222.
- 22 I. Sanchis, R. Spinelli, N. Aschemacher, M. V. Humpola and A. Siano, *Amino Acids*, 2020, **52**, 387–396.
- 23 G. L. Ellman, K. D. Courtney, V. Andres and R. M. Featherstone, *Biochem. Pharmacol.*, 1961, **7**, 88–95.
- 24 H. M. Greenblatt, G. Kryger, T. Lewis, I. Silman and J. L. Sussman, *FEBS Lett.*, 1999, **463**, 321–326.
- 25 S. N. Dighe, E. De la Mora, S. Chan, S. Kantham, G. McColl, J. A. Miles, S. K. Veliyath, B. Y. Sreenivas, Z. D. Nassar, I. Silman, J. L. Sussman, M. Weik, R. P. McGeary, M. O. Parat, X. Brazzolotto and B. P. Ross, *Commun. Chem.*, 2019, **2**, 1–14.
- 26 G. M. Morris, R. Huey, W. Lindstrom, M. F. Sanner, R. K. Belew, D. S. Goodsell and A. J. Olson, *J. Comput. Chem.*, 2009, **30**, 2785–2791.
- 27 D. A. Case, R. M. Betz, W. Botello-Smith, D. S. Cerutti, I. T. E. Cheatham, T. A. Darden, R. E. Duke, T. J. Giese, H. Gohlke, A. W. Goetz, N. Homeyer, S. Izadi, P. Janowski, J. Kaus, A. Kovalenko, T. S. Lee, S. LeGrand, P. Li, C. Lin, T. Luchko, R. Luo, B. Madej, D. M. York, P. A. K. M. York and P. A. Kollman, *Univ. California, San Fr.*, 2016, 10779586.
- 28 J. Wang, W. Wang, P. A. Kollman and D. A. Case, *J. Mol. Graphics Modell.*, 2006, **25**, 247–260.
- 29 W. D. Cornell, P. Cieplak, C. I. Bayly, I. R. Gould, K. M. Merz, D. M. Ferguson, D. C. Spellmeyer, T. Fox, J. W. Caldwell and P. A. Kollman, *J. Am. Chem. Soc.*, 1995, **117**, 5179–5197.
- 30 J. Wang, R. M. Wolf, J. W. Caldwell, P. A. Kollman and D. A. Case, *J. Comput. Chem.*, 2004, **25**, 1157–1174.
- 31 W. L. Jorgensen, J. Chandrasekhar, J. D. Madura, R. W. Impey and M. L. Klein, *J. Chem. Phys.*, 1983, **79**, 926–935.
- 32 S. Miyamoto and P. A. Kollman, *J. Comput. Chem.*, 1992, **13**, 952–962.
- 33 J. A. Izaguirre, D. P. Catarello, J. M. Wozniak and R. D. Skeel, *J. Chem. Phys.*, 2001, **114**, 2090.
- 34 U. Essmann, L. Perera, M. L. Berkowitz, T. Darden, H. Lee and L. G. Pedersen, *J. Chem. Phys.*, 1995, **103**(19), 8577–8593.
- 35 D. R. Roe and T. E. Cheatham, *J. Chem. Theory Comput.*, 2013, **9**, 3084–3095.
- 36 S. Genheden and U. Ryde, *Expert Opin. Drug Discovery*, 2015, **10**, 449–461.
- 37 M. J. Frisch, G. W. Trucks, H. B. Schlegel, G. E. Scuseria, M. A. Robb, J. R. Cheeseman, G. Scalmani, V. Barone, G. A. Petersson, H. Nakatsuji, X. Li, M. Caricato, A. V. Marenich, J. Bloino, B. G. Janesko, R. Gomperts, B. Mennucci, H. P. Hratchian, J. V. Ortiz, A. F. Izmaylov, J. L. Sonnenberg, D. Williams-Young, F. Ding, F. Lipparini, F. Egidi, J. Goings, B. Peng, A. Petrone, T. Henderson, D. Ranasinghe, V. G. Zakrzewski, J. Gao, N. Rega, G. Zheng, W. Liang, M. Hada, M. Ehara, K. Toyota, R. Fukuda, J. Hasegawa, M. Ishida, T. Nakajima, Y. Honda, O. Kitao, H. Nakai, T. Vreven, K. Throssell, J. Montgomery, Jr., J. E. Peralta, F. Ogliaro, M. J. Bearpark, J. J. Heyd, E. N. Brothers, K. N. Kudin, V. N. Staroverov, T. A. Keith, R. Kobayashi, J. Normand, K. Raghavachari, A. P. Rendell, J. C. Burant, S. S. Iyengar, J. Tomasi, M. Cossi, J. M. Millam, M. Klene, C. Adamo, R. Cammi,

- J. W. Ochterski, R. L. Martin, K. Morokuma, O. Farkas, J. B. Foresman and D. J. Fox, *Gaussian*, Gaussian, Inc., Wallingford CT, 2016.
- 38 R. F. W. Bader, *Acc. Chem. Res.*, 1985, **18**, 9–15.
- 39 T. Lu and F. Chen, *J. Comput. Chem.*, 2012, **33**, 580–592.
- 40 L. J. Gutiérrez, O. Parravicini, E. Sánchez, R. Rodríguez, J. Cobo and R. D. Enriz, *J. Biomol. Struct. Dyn.*, 2018, 1–18.
- 41 E. E. Barrera Guisasola, L. J. Gutiérrez, R. E. Salcedo, F. M. Garibotto, S. A. Andujar, R. D. Enriz and A. M. Rodríguez, *Comput. Theor. Chem.*, 2016, **1080**, 56–65.
- 42 L. J. Gutierrez, E. E. Barrera Guisasola, N. Peruchena and R. D. Enriz, *Mol. Simul.*, 2016, **42**, 196–207.
- 43 E. L. Angelina, S. A. Andujar, R. D. Tosso, R. D. Enriz and N. M. Peruchena, *J. Phys. Org. Chem.*, 2014, **27**, 128–134.
- 44 J. E. Ortiz, A. Garro, N. B. Pigni, M. B. Agüero, G. Roitman, A. Slanis, R. D. Enriz, G. E. Feresin, J. Bastida and A. Tapia, *Phytomedicine*, 2018, **39**, 66–74.
- 45 S. A. Andujar, R. D. Tosso, F. D. Suvire, E. Angelina, N. Peruchena, N. Cabedo, D. Cortes and R. D. Enriz, *J. Chem. Inf. Model.*, 2012, **52**, 99–112.